Modelling and simulation of an active fibre for cardiac muscle

P. Krejci* J. Sainte-Marie†‡ M. Sorine†
J.M. Urquiza§

CRM-3208

January 2006

*Mathematical Institute, Academy of Sciences of the Czech Republic, Žitná 25, 11567 Praha 1, Czech Republic, and Weierstrass Institute for Applied Analysis and Stochastics (WIAS), Mohrenstr. 39, 10117 Berlin, Germany, ✉ krejci@wias-berlin.de, krejci@math.cas.cz

†INRIA Rocquencourt, France ✉ Jacques.Sainte-Marie@inria.fr, ✉ Michel.Sorine@inria.fr

‡CETMEF/LNHE, Chatou, France

§Centre de recherches mathématiques, Université de Montréal, Canada ✉ urquiza@CRM.UMontreal.CA

Abstract

We present a mathematical model describing the electro-mechanical coupling and the mechanical activity of the myofibres of the cardiac muscle and we perform the simulations for the partial differential equations describing the dynamical displacement of a one-dimensional body with the resulting constitutive law. Prescribed boundary conditions describing the cardiac valves mechanisms and the arterial pressure variations are such that, by analogy, the whole model describes the electrically activated mechanical cardiac cycles.

1 Introduction

Despite its porosity and the blood veins system (coronary perfusion) that enters in its structural composition the cardiac muscle can be viewed as a continuum solid body. Like most soft biological tissues, the myocardium is a non-homogeneous and anisotropic material. Nevertheless, it is reasonable to assume that its mechanical behaviour is orthotropic and that the orthogonal directions are dictated by the fiber-sheet architecture of the myocardial tissue. These fibers are arranged in sheets: the first direction is along the muscle fibers, the second one is orthogonal to the fibers in the sheet plane and the third one is normal to the sheet plane. Except for some particular regions of the heart, the variations of the muscle fibers direction are generally smooth. This fibrous-sheet architecture has various consequences on the mathematical modelling [24] and on the experimental investigations aiming at characterizing the mechanical behaviour of the cadiac muscle [6]. *In vitro* multiaxial tests and *in vivo* minimally invasive or non-invasive techniques to measure stresses and relative strains, combined with the available microstructural data allow to derive suitable constitutive laws [16, 10].

In this paper we present the partial differential equations of a finite one-dimensional body with an electrically activated constitutive law derived from physiological considerations. This constitutive law is based on a recently developped model for the stress generation in the sarcomere, the muscle fiber micro-unit [5]. By a distribution moment technique which allows to obtain an active stress-strain law at the macroscopic scale, and by inserting this model into a rheological model of Hill-Maxwell type that allows to represent other characteristic behaviours of the cardiac muscle (isovolumetric contraction, passive viscoelasticity), we obtain a constitutive relation having the general form:

$$\Sigma(t) = \mu\varepsilon_t(t) + \mathcal{W}(\{\varepsilon(s); 0 \leq s \leq t\}) \tag{1}$$

In this relation, Σ and ε denote respectively the stress and the strain in the axial direction of the fibre and μ is a positive viscosity parameter that accounts for the viscosity due to the fluid that is part of the composition of the myocardium. Subscript t indicates the time (partial) derivative.

Here, $\mathcal{W}$ is a stress component which at every time t depends on the history of the strain from the reference time $t = 0$. It depends also on the initial values of internal variables. It is a *memory* operator and classical models of solid mechanics in differential or integral form including differential or integral viscoelastic, elasto-visco-plastic and more generally inelastic models can be represented in this way [1, 7, 21, 26]. Finally, it also depends on the time-varying electrical excitation.

Assuming small displacements, the strain in the axial direction can be written $\varepsilon(x,t) = y_x(x,t)$ where $y(x,t)$ is the longitudinal displacement of each material point of the physical fiber from the reference configuration $y(x,0) = y^{\text{ref}}(x,0) = 0$, $0 \leq x \leq \ell$, ℓ being the length of the fiber in the reference configuration.

The conservation of momentum equation governing the longitudinal fiber displacements thus has the form:

$$y_{tt}(x,t) = \Sigma_x(x,t), \qquad 0 \leq x \leq \ell, \quad t \geq 0. \tag{2}$$

In [16], we investigated the existence, uniqueness, as well as the asymptotic behavior of solutions to (1)-(2) for a physiologically based constitutive law of cardiac fibers. Here, we focus on the modelling aspect. Details are given about the derivation of this constitutive law and a modification is introduced in order to be compatible with the Frank-Starling law. Then we test it numerically, showing its ability to reproduce cardiac mechanical cycles under electrical excitations both in normal and pathological situations.

The remaining of the article is organized as follows. In the next section we describe the constitutive law and its physiological foundations as well as the electrical input signal that activates the contraction of the cardiac fibers. In other words, we specify $\mathcal{W}$ in (1), and thus Σ in (2). Then, in section 3, we construct a one space-dimensional mechanical model that analogically describes the contraction of the cardiac left ventricule. Cardiac valves mechanism as well as the interaction with

the arterial blood are modeled resulting in a particular boundary condition for the one-dimensional partial differential equation (2) previously obtained. Finally, simulations based on the discretization of the resulting initial-boundary value problem are presented in section 4 and the results are discussed in view of the ability of the model to reproduce realistic cardiac mechanical cycles.

2 Excitation-contraction modeling

In this section we present the electrically activated constitutive law for the cardiac muscle along the direction of each fiber, which means that the local stress along the direction of the local fiber is expressed in terms of the strain along this direction. We first recall the model for the contractile stress-strain law introduced in [5] (see also [4]) for cardiac fibers. Then, this excitation-contraction coupling law is modified in order to account for the well known Frank-Starling regulatory mechanism of the cardiac muscle. We also characterize the electrical activity that generates this active component of the mechanical stress. Finally, the resulting active stress-strain law is inserted in a rheological model so as to account for passive relaxation and isovolumetric phases of the cardiac mechanical cycle.

2.1 The electrical excitation-contraction coupling

It is commonly admitted that the model of actin-myosin bridge dynamics due to Huxley [13] allows to describe the muscle-contraction phenomena at the sarcomere scale. Furthermore, Zahalak [30] has shown how the method of moments can be applied to this model in order to describe muscle-contraction on the myofibre scale. Nevertheless, the attachment and detachment rates of the bridges are still the object of heuristic modeling and experimental testing aiming at recovering some mechanical properties of the myocardium, directly at the macroscopic level [12], and at identifying the attachment and detachment rates of the bridges [29]. By contrast, the model that we use is formulated with a constitutive law based on physical considerations prevailing at the sarcomere scale. We recall this model briefly.

On a microscopic scale, the sarcomere is made up of thin and thick parallel filaments. When ATP (the fuel of the cell) is available and the level of intracellular calcium bound on troponin C (the control of the contraction and relaxation in the sarcomeres) reaches a threshold ($Ca_{TnC} \geq \bar{C}$), the myosin heads of the thick filament that are not too far from actin sites on the thin filament ($\xi \in [0,1]$ for some microscopic strain), become likely to bind with the binding rate f.

Unbinding is due to the macroscopic strain rate ε_t^c, or to the action of the calcium pumps under the threshold $\bar{C}$, or to large values of ξ. The unbinding rate is g. The previous conditions are translated into the following formulae (where $\mathbb{I}_S$ is the characteristic function of the set S) [5]:

$$\begin{aligned} f(\xi,t) &= k_{ATP}.\mathbb{I}_{Ca_{TnC}\geq\bar{C}}.\mathbb{I}_{\xi\in[0,1]}, \\ g(\xi,t) &= \alpha|\varepsilon_t^c| + k_{SR}.\mathbb{I}_{Ca_{TnC}<\bar{C}} + k_{ATP}.\mathbb{I}_{Ca_{TnC}\geq\bar{C}}.\mathbb{I}_{\xi\notin[0,1]}. \end{aligned}$$

The parameter k_{ATP} represents the rate of the chemical reaction providing energy from the hydrolysis of ATP to the molecular motors in the sarcomere, whereas k_{SR} denotes the rate of bridge destruction due to sarcoplasmic reticulum pumps removing calcium ions from the troponin. The parameter α is dimensionless and positive.

It will be convenient to define a new control variable

$$u(t) = k_{ATP}.\mathbb{I}_{Ca_{TnC}(t)\geq\bar{C}} - k_{SR}.\mathbb{I}_{Ca_{TnC}(t)<\bar{C}}$$

so that $f(\xi,t) = |u(t)|_+.\mathbb{I}_{\xi\in[0,1]}$ and $f(\xi,t) + g(\xi,t) = \alpha|\varepsilon_t^c| + |u(t)|$ where $|u|_+ = \max(0,u) = k_{ATP}.\mathbb{I}_{Ca_{TnC}(t)\geq\bar{C}}$ and $|u|_- = \max(0,-u) = k_{SR}.\mathbb{I}_{Ca_{TnC}(t)<\bar{C}}$ are ATP consumption rates during contraction and active relaxation respectively.

The interaction potential W^{am} of the actin-myosin system is responsible for muscle contraction corresponding to the negative values of the macroscopic strain ε^c describing the relative sliding of the actin over the myosin filament. Let $n(\xi,t)$ be the density of cross-bridges with strain ξ at time t. Then, Huxley's model is:

$$n_t + \varepsilon_t^c\, n_\xi = (1-n)f - ng, \quad \sigma^c(t) = -d(\varepsilon^c)\int_{-\infty}^{+\infty} \frac{\partial W^{am}}{\partial \xi} n d\xi + \mu_c \varepsilon^c.$$

A parabolic W^{am} is chosen in [5]: $-\frac{\partial W^{am}}{\partial \xi} = k_0\xi_0 + \sigma_0\xi$. The parameters k_0 and σ_0 are strictly positive and related to the number and stiffness of available actin-myosin cross-bridges in the sarcomere, μ_c is a viscosity parameter and ξ_0 is a strain constant. The scaling technique to compute σ^c leads to introduce k^c and τ^c, respectively proportional to the zero and first-order moments of n:

$$k^c(t) = k_0 \int_{-\infty}^{+\infty} n(\xi,t)d\xi \quad \text{and} \quad \tau^c(t) = \sigma_0 \int_{-\infty}^{+\infty} \xi n(\xi,t)d\xi.$$

The resulting constitutive relation is given by the following system of ordinary differential equations:

$$\left\{ \begin{array}{ll} \tau_t^c = k^c\varepsilon_t^c - (\alpha|\varepsilon_t^c| + |u|)\tau^c + \sigma_0|u|_+, & \tau^c(0) = \tau_0^c, \\ k_t^c = -(\alpha|\varepsilon^c| + |u|)k^c + k_0|u|_+, & k^c(0) = k_0^c, \\ \sigma^c = d(\varepsilon^c)(\tau^c + k^c\xi_0) + \mu_c\varepsilon_t^c, & \end{array} \right. \tag{3}$$

where u denotes the electrical input – corresponding to a normalized concentration of calcium bound on the troponin-C – with $u > 0$ during contraction and $u < 0$ during active relaxation. The modeling of u is further elaborated in Section 2.3 and the meaning of $d(\varepsilon^c)$ is discussed in the next section.

Without entering in a detailed analysis (which is done in [4] for a similar system of ordinary diffenrential equations and in [16] for the partial differential equations using this constitutive law), let us just point out some abilities of the model:

- *Active contraction.* If the initial contractile stress τ^c is relatively small then for positive u, this stress increases monotonically.
- *Active relaxation.* For negative u, the contractile rigidity k^c decreases, and τ^c can reasonably be expected to decrease too.

The thermomechanical compatibility of this constitutive law is discussed in section 2.4.

2.2 Starling effect

The Starling effect is one of the most important regulatory mechanisms of the heart activity. By this mechanism, when the preload increases the heart is able to also increase its contraction. The preload corresponds to the stretching of the cardiac fibres at the end of the previous diastolic filling, hence it is related to the veinous return and the pressure in the atria. Thus, increasing the ventricular end-diastolic pressure leads to an increased stroke volume, see Fig. 1. The Starling effect can also be interpreted by saying that the heart adapts its contraction so that the stroke volume compensates the end-diastolic volume.

The underlying physiological mechanism is as follows. When the stretching of the sarcomere increases, the troponin-C calcium sensitivity also increases leading to a growth of the cross-bridge attachment availability. This means that when the stretching of the sarcomere increases we move from point (a) to (b) on the curve presented in Fig. 2-(i), in which I denotes the normal range for the sarcomere length. This phenomenon is no more valid for very large stretching of the sarcomere, as represented by (c) in the figure. These various states of deformation are also schematically depicted in Fig. 3. It appears that for large deformations fewer actin-myosin cross-bridges can be created. This leads to the factor $d(\varepsilon^c)$ introduced in [19]. This factor is a function with values in the interval $[0,1]$ and behaving as represented in Fig. 2-(ii).

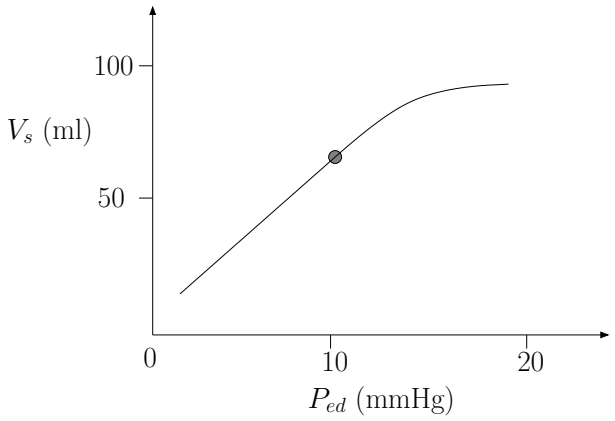

Figure 1: The Franck-Starling curve. V_s: stroke volume ; P_{ed}: left ventricular end-diastolic pressure.

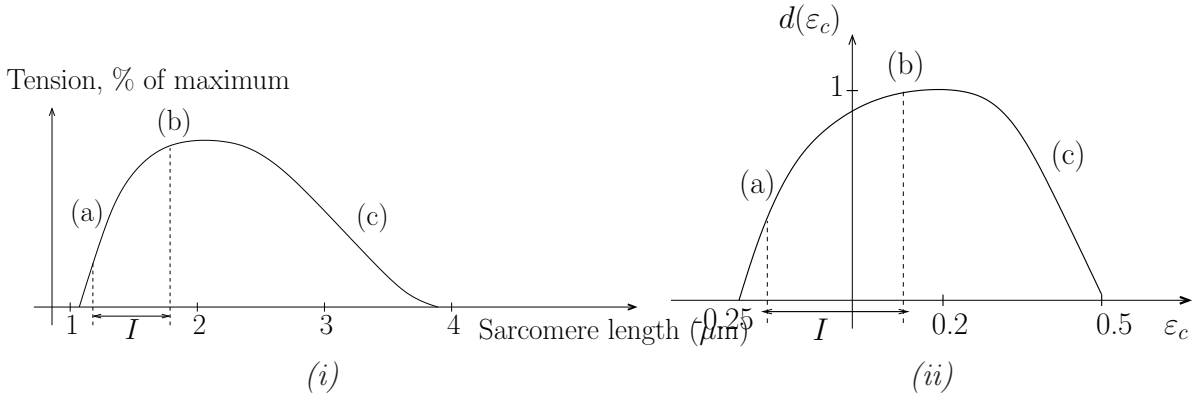

(i) *(ii)*

Figure 2: *(i)* the "length-tension" curve of a muscle with the three different configurations of the sarcomere given in Fig. 3 (see [14]) and *(ii)* the corresponding modulation $d(\varepsilon^c)$ of the active stress σ^c.

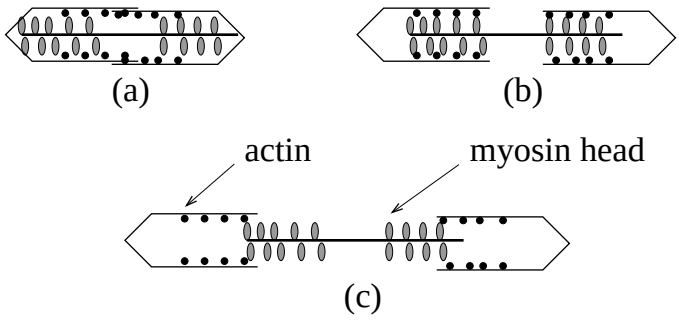

Figure 3: Three different sarcomere deformations.

2.3 Electrical activation

The propagation of the action potential v in the cardiac tissue results from the diffusion of calcium, sodium and potassium ions in the extracellular space, from ionic currents through the cell membrane and from reactions of these ions in the intracellular space. There are many different types of ionic channels (and corresponding current models), some of them having an open/closed state modeled by gate variables. Let I_{ion} be the total equivalent electrical current through the membrane. In the intracellular space the reactions involve the concentrations of calcium bound on various proteins, in particular troponin-C that regulates Ca^{2+} induced muscle contraction, as already mentioned. Let w be the vector of all concentrations and ionic gating variables involved in the intracellular reactions and ionic channels. Then the general mono-domain model for v is a reaction-diffusion equation for v coupled with an ODE for w (see e.g. [15] and references therein), as represented in the following system where I_{ext} denotes a stimulation current, c_m, $\underline{\underline{\sigma}}_m$ are given scalar capacitance and conductivity tensor:

$$\begin{cases} c_m v_t - \mathrm{div}(\underline{\underline{\sigma}}_m.\underline{\nabla} v) + I_{ion}(v,w) = I_{ext} \ \text{ in } \Omega_H, \\ w_t - R(v,w) = 0 \ \text{ in } \Omega_H, \\ \nu^T.(\underline{\underline{\sigma}}_m \underline{\nabla} v) = 0 \ \text{on } \partial\Omega_H, \end{cases} \tag{4}$$

where Ω_H denotes the heart tissue domain and $\partial\Omega_H$ its boundary with unit outward normal vector $\underline{\nu}$. Remark that in bidomain models an external potential and an external conductivity are also considered, leading to a slight modification of (4), see [15, 20].

In our simulations we have used a very simple monodomain model, a variant of the two-variable FitzHugh-Nagumo model proposed by Aliev and Panfilov [2], where w is a scalar "repolarization potential":

$$\begin{cases} c_m I_{ion}(v,w) = kv(v-a)(v-1) + vw, \\ R(v,w) = \varepsilon(v,w)(-w - kv(v-a-1)), \end{cases} \tag{5}$$

where $\varepsilon(v,w) = \varepsilon_0 + \mu_1 w/(v+\mu_2)$ and σ_m/c_m, k, a, ε_0, μ_1, μ_2 are positive parameters. This model is able to generate v-traveling waves sufficiently realistic for our purpose, i.e. simulating isolated heart beats in various conditions. For a series of heart beats it would be necessary to consider a more realistic calcium dynamics than the simple w-repolarization dynamics. Nevertheless, we need an output variable similar to Ca_{TnC}, an output available only in models with higher dimensional w, as e.g. in [9]. Note that, given a realistic v-traveling wave – e.g., generated by (5) – it is possible to use it as the input of a more complete ODE of the form $w_t - R(v,w) = 0$ to generate a w-traveling wave and then to estimate the desired output. Remark also a drawback of this heuristic approach: it is difficult to take into account possible mechano-electric feedback loops, as e.g. the dependence of the rate of Ca-detachment from troponin-C upon the sarcomere tension (or stretch rate) [11], which we do not consider here. In fact, in our heart model we have used (5) with a simple affine relation between u and v: $u = h(v - \bar{v})$. This approach is substantiated by the similitude of the v and Ca_{TnC} waveforms obtained with the more refined model of [9], as shown in Figure 4.

Finally, we have considered several types of activation models:

- A uniform activation without propagation, $u(M,t) \equiv u(t)$ for all points M of the muscle.
- A simplified propagation mechanism with $u(M,t) = h(v^*(t - \Pi M/c) - \bar{v})$ where v^* is an action potential template, ΠM is the projection of M along the apex to the base axis and c is the velocity of the wavefront.
- A traveling wave generated with a reaction-diffusion model as described above.

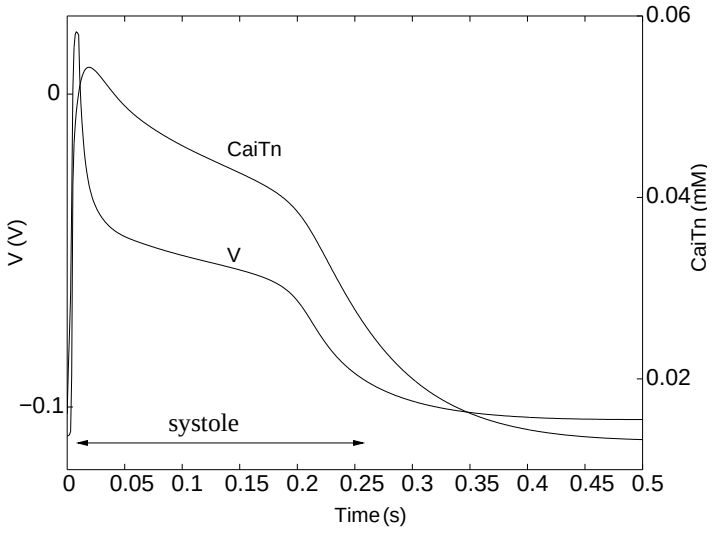

Figure 4: Responses of the action potential v and concentration of calcium buffered on troponin-C (Ca_{TnC}) for an external stimulation current I_{ext} modeled as an impulse at time 0 (taken from [9]).

2.4 The Hill-Maxwell rheological model

The myofibre constitutive law described above is now incorporated in a rheological model of Hill-Maxwell type [8], as depicted in Figure 5. The element E_c accounts for the contractile electrically-activated behavior governed by (3) and each variable appearing with superscript c refers to this element. Elastic material laws are used for the series and parallel elements E_s and E_p. Based on experimental results, the corresponding stress-strain laws are generally assumed to be of exponential type for E_p, and linear for E_s [18, 28, 25]. The role of E_p is to prevent the heart from overstepping certain limits during filling or ejection, while E_s and E_c allow the contraction and the active relaxation.

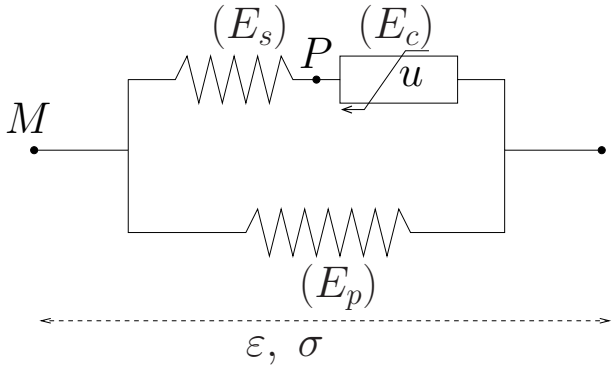

Figure 5: Hill-Maxwell rheological model.

The degree of freedom between E_c and E_s, i.e. the point P on Fig. 5, allows to represent the isovolumetric phases during the cardiac cycle. The equilibrium relations in the two branches ensure that

$$\sigma = \sigma^p + \sigma^c \quad \text{and} \quad \sigma^c = \sigma^s,$$

with $\sigma^p = f_p(\varepsilon)$ and $\sigma^c = E_s\varepsilon^s = E_s(\varepsilon - \varepsilon^c)$. The total strain is additively composed by the deformations corresponding to the series and contractile elements respectively i.e. $\varepsilon = \varepsilon^c + \varepsilon^s$. Insertion of the constitutive law for the contractile element into this Hill-Maxwell rheological model with aforementioned elastic laws for the series and parallel elements give the following set of equations

that define the constitutive law for a cardiac fibre:

$$\left\{\begin{array}{l} \tau_t^c = k^c\varepsilon_t^c - (\alpha|\varepsilon_t^c| + |u|)\,\tau^c + \sigma_0 u^+, \\ k_t^c = -\,(\alpha|\varepsilon_t^c| + |u|)\,k^c + k_0\,u^+, \\ \mu_c\varepsilon_t^c = E_s(\varepsilon - \varepsilon^c) - d(\varepsilon^c)\tau^c, \\ \sigma = f_p(\varepsilon) + E_s(\varepsilon - \varepsilon^c). \end{array}\right. \tag{6}$$

Recall that we assume that μ_c is strictly positive. As a result, ε being given in $]0, +\infty[$, internal variables ε^c, k^c and τ^c are obtained by solving the first three differential equations of (6) and are uniquely defined if initial conditions are prescribed:

$$\varepsilon^c(0) = \varepsilon^{oc},\ k^c(0) = k^{oc},\ \tau^c(0) = \tau^{oc}.$$

Then σ is an ouput given by the algebraic relation $\sigma = f_p(\varepsilon) + E_s(\varepsilon - \varepsilon^c)$.

If $\mu_c = 0$ then the third equation in (6) is purely algebraic. In this case, the system of differential-algebraic equations (6) would require initial data to be provided for k^c and τ^c, and the initial data for ε^c should satisfy the third equation of (6) so as to have smooth solutions. This case is not considered in this work.

It is easy to verify that due to the thermo-mechanical compatibility of the contractile element E_c [16, 22] and of the series and parallel element, the Hill-Maxwell rheological model constitued with these elements is thermo-mechanically compatible as well. Indeed, a straightforward calculus (see [16, 22]) gives

$$\sigma\,\varepsilon_t^c = \frac{d}{dt}\left(\frac{d(\varepsilon^c)(\tau^c)^2}{2k^c}\right) + \mu_c(\varepsilon_t^c)^2 + (\alpha|\varepsilon_t^c| + |u|)\frac{d(\varepsilon^c)(\tau^c)^2}{2k^c} + u^+ d(\varepsilon^c)\left(\frac{k_0}{2}\left(\frac{\tau^c}{k^c}\right)^2 - \sigma_0\,\frac{\tau^c}{k^c}\right) - \varepsilon_t^c d'(\varepsilon^c)\frac{(\tau^c)^2}{2k^c},$$

as well as

$$\begin{aligned} \sigma\,\varepsilon_t \;=\; & \frac{d}{dt}\left(F_p(\varepsilon) + \frac{E_s}{2}(\varepsilon - \varepsilon^c)^2 + \frac{d(\varepsilon^c)(\tau^c)^2}{2k^c}\right) + \mu_c(\varepsilon_t^c)^2 + \\ & (\alpha|\varepsilon_t^c| + |u|)\frac{d(\varepsilon^c)(\tau^c)^2}{2k^c} + u^+ d(\varepsilon^c)\left(\frac{k_0}{2}\left(\frac{\tau^c}{k^c}\right)^2 - \sigma_0\,\frac{\tau^c}{k^c}\right) - \varepsilon_t^c d'(\varepsilon^c)\frac{(\tau^c)^2}{2k^c} \end{aligned} \tag{7}$$

where $F_p(\varepsilon) := \int_0^\varepsilon f_p(z)\,dz$. When there is no electrical activation ($u = 0$) it has the form

$$\sigma\,\varepsilon_t \;=\; \frac{d}{dt}\mathcal{U}(t) + \mathcal{P}(t), \tag{8}$$

with

$$\begin{aligned} \mathcal{U}(t) \quad &= \left(F_p(\varepsilon) + \tfrac{E_s}{2}(\varepsilon - \varepsilon^c)^2 + \tfrac{d(\varepsilon^c)(\tau^c)^2}{2k^c}\right), \\ \mathcal{P}(t) \quad &= \mu_c(\varepsilon_t^c)^2 + \alpha|\varepsilon_t^c|\tfrac{d(\varepsilon^c)(\tau^c)^2}{2k^c} - \varepsilon_t^c d'(\varepsilon^c)\tfrac{(\tau^c)^2}{2k^c}. \end{aligned}$$

Here, $\mathcal{U}$ is a free energy and $\mathcal{P}$ the dissipation rate which, according to the second law of thermodynamics, must be non-negative. This condition is for instance ensured under our assumption that α and d satisfy $\alpha d(\varepsilon^c) \geq |d'(\varepsilon^c)|$ for ε^c in the expected physical range I (see section 2.2).

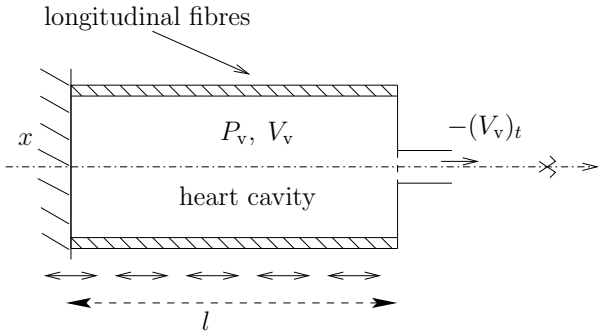

Figure 6: One-dimensional analogy. $P_{\rm v}$ and $V_{\rm v}$ respectively denote the pressure and the volume of the cavity.

3 A one-dimensional mechanical model for cardiac contractions

Using an analogy of the left ventricule behaviour with a cylinder with varying length and constant (in space and time) section (see Fig. 6), we obtain a one-dimensional mechanical model for the left ventricular contractions with the constitutive law (3). For a description of a complete three-dimensional model of the cardiac mechanical behaviour incorporating the excitation-contraction law described in this paper we refer to [8].

Additional viscous effects due to the fluid component of the heart body are considered through the addition of a viscous damping in parallel with element E_p. This leads to the following governing equations

$$\varrho y_{tt}(x,t) - (\mu\varepsilon_t(x,t) + \sigma(x,t))_x = 0, \quad \text{for } (x,t) \text{ in }]0,\ell[\times]0,+\infty[, \tag{9}$$

where $\mu > 0$ is the corresponding viscosity parameter, ϱ is a mass density, ℓ is the length of the reference cavity and σ is the stress component along the x-axis, governed by the constitutive law (6). Here $y(x,t)$ denotes the displacement along the x-axis and $\varepsilon(x,t)$ the corresponding strain, namely

$$\varepsilon(x,t) = y_x(x,t). \tag{10}$$

We consider that the stress-strain law $\varepsilon \mapsto f_p(\varepsilon)$ is continuous, of exponential type for moderate strains but with linear growth for large strains:

$$f_p(\varepsilon) = \begin{cases} \lambda_1(e^{\beta_1(\varepsilon-\bar\varepsilon_1)} - 1) - \lambda_2(e^{-\beta_2(\varepsilon-\bar\varepsilon_2)} - 1) & \text{for} \quad |\varepsilon| \le \varepsilon^{max}, \\ \text{affine in } \varepsilon \text{ elsewhere,} \end{cases} \tag{11}$$

where $\beta_1 > 0$, $\beta_2 > 0$, $\bar\varepsilon_1$ and $\bar\varepsilon_2$ are constant parameters, indepedant of x. Due to its behaviour for large strains f_p satisfies the assumption under which the existence and uniqueness result in [16] is proved. Let us also note that in our performed computations $|\varepsilon(x,t)| \le \varepsilon^{max}$ for the chosen ε^{max}, so that its linearity assumption for large strains is not necessary for our computations.

The time-dependent activation quantity $u(x,t)$ appears as a desired shortening velocity (the usual interpretation of calcium concentration near troponin C sites) or output flow. As described in section 2.3, u has the form

$$u(x,t) = h\,\theta(x)\,(v^*(t - x/c(x)) - \bar v) \tag{12}$$

where $c(x) = c_0 > 0$ and $\theta(x) = 1$, $0 \le x \le \ell$, in a reference case whereas $c(x)$ and $\theta(x)$ can vary with x in pathological cases. The T-periodic function v^* is the one plotted in Fig.4 over one period.

We now model the coupling between the ventricle and the circulatory system. It invokes the blood pressure in the cavity, $P_{\rm v}(t)$, the blood pressure in the aorta, $P_{\rm ar}(t)$, the mitral pressure $P_{\rm at}(t)$ and the volume of the cavity $V_{\rm v}(t)$ (see figure 7-a, where we consider that the aortic valve and the mitral valve overlap). Let us also introduce the blood flow from the left ventricule through the aortic valve, defined by

$$q = -(V_{\rm v})_t. \tag{13}$$

The flow q is related to the displacements field by $q = -Sy_t(\ell, t)$, S being the section of the deformable piston (see Fig 6).

The mechanism regulating the opening and closure of the valves and the evolution of the aortic pressure are described in the two following subsections.

3.1 Opening and closure of the valves

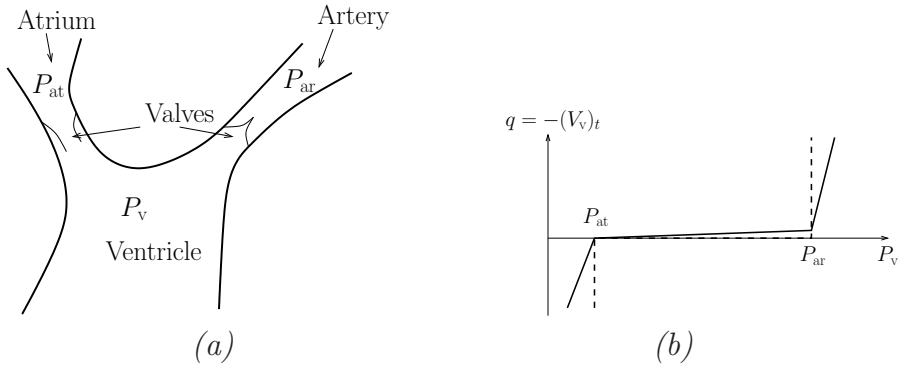

Figure 7: Aortic valve model, *(a)* mecanism and *(b)* formulation as a contact problem, (- -) relation (14) and (–) relation (16).

The aortic valve opens when $P_{\rm v} = P_{\rm ar}$ whereas the mitral valve opens when $P_{\rm v} = P_{\rm at}$. Thus the boundary conditions can be formulated as the following double contact problem:

$$\left\{ \begin{array}{ll} q \leq 0 & \text{when } P_{\rm v} = P_{\rm at} \quad \text{(filling)} \\ q = 0 & \text{when } P_{\rm at} < P_{\rm v} < P_{\rm ar} \quad \text{(isovolumetric phases)} \\ q \geq 0 & \text{when } P_{\rm v} = P_{\rm ar} \quad \text{(ejection)} \end{array} \right. \tag{14}$$

This formulation fully describes the blood flow through the valves but, since relation (14) is not regular during the isovolumetric phases, we prefer a regularized version satisfying $\frac{dq}{dP_{\rm v}} > 0$ for every $P_{\rm v}$, see Fig. 7-b. During isovolumetric phases we also want $\frac{dq}{dP_{\rm v}} \ll 1$. Due to the blood viscosity we consider that during ejection the blood flow is proportional to the difference of pressure $P_{\rm v} - P_{\rm ar}$ (see [17]) leading to $q = K_{\rm ar}(P_{\rm v} - P_{\rm ar})$ with

$$K_{\rm ar} = \frac{\pi R^2}{\varrho_b c}, \tag{15}$$

R being the radius of valve, ϱ_b the blood density and c the velocity of wave propagation. During the filling one has similarly $q = K_{\rm at}(P_{\rm v} - P_{\rm at})$ with $K_{\rm at} \approx K_{\rm at}$. Finally in accordance with the requirements mentionned above, we choose the folowing regularized version of (14):

$$\left\{ \begin{array}{ll} q = K_{\rm p}(P_{\rm v} - P_{\rm at}), & \text{when } P_{\rm at} \leq P_{\rm v} \leq P_{\rm ar}, \\ q = K_{\rm ar}(P_{\rm v} - P_{\rm ar}) + K_{\rm p}(P_{\rm ar} - P_{\rm at}), & \text{when } P_{\rm v} \geq P_{\rm ar}, \\ q = K_{\rm at}(P_{\rm v} - P_{\rm at}), & \text{when } P_{\rm v} \leq P_{\rm at}, \end{array} \right. \tag{16}$$

where $0 < K_{\rm p} \ll K_{\rm ar}$ and $K_{\rm p} \ll K_{\rm at}$. Using (13), the previous relation is simply denoted by

$$-(V_{\rm v})_t = f(P_{\rm v}, P_{\rm ar}, P_{\rm at}). \tag{17}$$

3.2 Windkessel model

In order to obtain realistic behaviour of the model during systole, it is necessary to model the external blood circulation and thus to consider that P_{ar} vary along the cardiac cycle and especially during the ejection. To this end we consider that P_{ar} is governed by a Windkessel type model.

Windkessel and similar lumped models are often used to represent blood flow and pressure in the arteries. These models can be derived from electrical circuit analogies where current represents arterial flow and voltage represents arterial pressure. For more information about Windkessel models of blood flow in arteries, one can refer to [3, 27, 23].

The 3-element Windkessel model is governed by:

$$C(P_{\text{ar}})_t + \frac{P_{\text{ar}} - P_{\text{sv}}}{R_p} = (1 + \frac{R_c}{R_p})q^+ + CR_c q_t \mathbb{I}_{q^+} \tag{18}$$

where P_{ve} is the venous pressure, R_p the peripheral resistance in the systemic or pulmonary circuit, C the arterial compliance and R_c the arterial resistance. The right-hand side of (18) is nonzero only during the ejection phase, i.e. when $q > 0$. In Fig. 8, the arrows for C and R_p indicate that these quantities can be functions of P_{ar}.

In the cavity, q being given by $-(V_{\text{v}})_t = q = f(P_{\text{v}}, P_{\text{ar}}, P_{\text{at}})$, Eq. (18) implies that the derivative of the displacement for the intraventricular cavity has to be calculated up to the second order. Since the mechanical model of the muscle has few inertia and damping, numerical difficulties may arise and we neglect the aortic resistance i.e. $R_c = 0$ in Eq. (18).

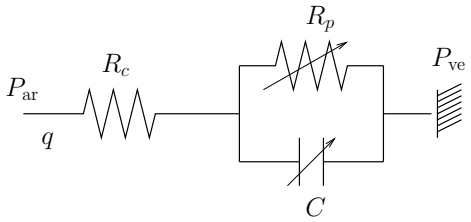

Figure 8: The 3-element Windkessel model.

Whereas the blood pressure in each artery i.e. P_{ar} is an output of the model, the pressure in each atrium P_{at} is given and synchronized with the activation u. For the atrium contraction, we propose the following modelling. During systole (Fig. 4), P_{at} is almost constant i.e. $P_{\text{at}}(t) \approx P^0_{\text{at}}$ and the atrium contraction during the diastolic phase is represented by an increase δP^0 of the blood pressure in the atrium. Thus the variations of P_{at} over a sequence of cardiac cycles can be represented by the first order ordinary differential equation,

$$\begin{cases} (P_{\text{at}})_t = \frac{P^0_{\text{at}} + \delta P^0 \mathbb{I}_{I^c} - P_{\text{at}}}{\tau}, \\ P_{\text{at}}(0) = P^0_{\text{at}}, \end{cases}$$

where $I^c = \cup_{k=1}^{N} [I^c_0 + kT, I^c_1 + kT]$ denotes the time intervals where the auricular contraction occur. T is the length of a heart beat, N is the number of simulated heart beats, δP^0 is the desired increase of blood pressure in the atrium due to the contraction and τ is a time constant.

3.3 Problem formulation

From (6) and (9), the problem (P) to solve can be writen under the form

$$\begin{aligned} \varrho y_{tt} &= (\mu\varepsilon_t + \sigma)_x\,, && (19)\\ \varepsilon &= y_x\,, && (20)\\ \sigma &= f_p(\varepsilon) + E_s(\varepsilon - \varepsilon^c)\,, && (21)\\ \mu_c\varepsilon^c_t &= E_s(\varepsilon - \varepsilon^c) - d(\varepsilon^c)\tau^c\,, && (22)\\ \tau^c_t &= k^c\varepsilon^c_t - (\alpha|\varepsilon^c_t| + |u|)\tau^c + \sigma_0 u^+\,, && (23)\\ k^c_t &= -(\alpha|\varepsilon^c_t| + |u|)k^c + k_0 u^+ && (24) \end{aligned}$$

in the domain $(x,t) \in Q :=]0,\ell[\times]0,\infty[$ where u is given by (12). The couplings between the pressures in the artery, the atrium and the ventricle are given by

$$\left\{ \begin{array}{l} -Sy_t(\ell,t) = f(P_{\rm v}, P_{\rm ar}, P_{\rm at}) \\ C(P_{\rm ar})_t + \frac{P_{\rm ar}-P_{\rm sv}}{R_p} = (f(P_{\rm v}, P_{\rm ar}, P_{\rm at}))^+\,. \end{array} \right. \tag{25}$$

We need now to prescribe the boundary conditions. At $x = 0$, which plays the role of the apex, the elastic cavity is considered to be fixed:

$$y(0,t) = 0, \quad t > 0, \tag{26}$$

and we consider that the stress at $x = \ell$ equals the blood pressure in the artery. Thus the boundary condition at the base of the myocardium is

$$(\sigma + \mu\varepsilon_t)(\ell,t) = P_{\rm v}(t), \tag{27}$$

meaning that it is coupled with the Windkessel and valve models (25). Initial conditions for the displacement, the velocity and the internal variables need also to be prescribed, namely:

$$y(x,0) = y^o(x),\ y_t(x,0) = y^1(x), \tag{28}$$

$$\varepsilon^c(x,0) = \varepsilon^{oc}(x),\ k^c(x,0) = k^{oc}(x),\ \tau^c(x,0) = \tau^{oc}(x). \tag{29}$$

In [16], the existence and uniqueness of a solution to this problem is proved when $d(\varepsilon^c)$ is kept constant, with a boundary condition at the base of the myocardium taking the form:

$$(\sigma + \mu\varepsilon_t)(\ell,t) + \gamma(y_t(\ell,t)) = \psi(t),$$

for suitable functions γ and ψ.

4 Simulations

For the space discretization we use P_1 finite elements for the displacement field y and P_0 for the other variables. The equilibrium equation (19) is time-discretized using the $(\frac{1}{2},\frac{1}{4})$-Newmark scheme. All other ordinary differential equations describing the state variables are discretized using a mid-point scheme i.e.

$$\begin{aligned} f^{(t+\frac{\Delta t}{2})} &\approx (f^{(t+\Delta t)} + f^{(t)})/2,\\ (f_t)^{(t+\frac{\Delta t}{2})} &\approx (f^{(t+\Delta t)} - f^{(t)})/\Delta t. \end{aligned}$$

Application of the mid-point scheme to the Windkessel model (25)-(b) leads to

$$P_{\rm ar}^{(t+\Delta t)} - P_{\rm ar}^{(t)} + \frac{\Delta t}{C}\left(\frac{\frac{1}{2}(P_{\rm ar}^{(t+\Delta t)} + P_{\rm ar}^{(t)}) - P_{\rm sv}}{R_p} - \mathbb{I}_{P_{\rm ar}\geq P_{\rm v}}^{(t+\frac{\Delta t}{2})}\left(\frac{q^{(t+\Delta t)} + q^{(t)}}{2}\right)\right) = 0, \tag{30}$$

where $\mathbb{I}_{P_{\rm ar}\geq P_{\rm v}}^{(t+\frac{\Delta t}{2})}$ is 1 when $P_{\rm ar}^{(t+\frac{\Delta t}{2})} \geq P_{\rm v}^{(t+\frac{\Delta t}{2})}$ and 0 otherwise. Using (25)-(a) the flow is related to the internal volume (hence to the displacements) by

$$V_{\rm v}^{(t+\Delta t)} - V_{\rm v}^{(t)} + \frac{\Delta t}{2}(q^{(t+\Delta t)} + q^{(t)}) = 0. \tag{31}$$

At $t = 0$ we assume a steady state (end of diastole), where $P_{\rm ar} = 70$ mmHg and thus $q^{(0)} = 0$.

The numerical scheme allows to obtain explicit expressions of all state variables appearing in the contraction law (3) as functions of ε^c, namely, τ^c and k^c at time step $t + \Delta t$ are expressed in terms of ε^c at time step $t + \Delta t$ and of the state variables at time step t. Therefore, the time discretization leads to a non-linear problem in y, ε^c and $P_{\rm ar}$ for each time step, which is solved with a Newton method.

4.1 Reference situation

Simulations of the above model have been carried out, and the results obtained – in particular stresses, strains and pressures – correspond reasonably well to heart physiology. In Fig. 9 these global indicators for the cardiac function in a reference situation are presented.

Starting from realistic initial conditions, the simulations depicted in Fig. 9 correspond to the fourth cardiac cycle. The stability of the model is numerically demonstrated by results obtained over a sequence of cycles, which show that the system rapidly reaches an attractor (limit cycle). Changes in the initial data or modifications of the parameters values at a given time, as illustrated in Fig. 10, lead to a new limit cycle.

The values of the parameters used for the reference simulation are given in table 1. The shape v^* of the activation is the one depicted in Fig. 4.

4.2 Pathological cases

We now consider the case when the contractility σ_0 is reduced in a given area of the piston, as depicted in Fig. 11. Results of the corresponding simulations are compared with those obtained in the reference situation in Fig. 12. This pathology of σ_0 induces a decrease of the cardiac activity.

Dysfunctions of the cardiac activity can also be the consequence of troubles in the electrical activity. This is what we consider now. As mentionned in subsection 2.3, we assume that the action potential $u = u(x, t)$ has the form:

$$u(x, t) = h\,\theta(x)\,(v^*(t - x/c_1) - \bar{v})$$

with $c_1 = \frac{c_0}{2}$ and where $\theta(x) = 1 - \frac{x}{\ell}$ depends on x, see Fig. 13. Fig. 14 depicts the obtained results in such a pathological situation.

Due to the form of Eqs. 3 where σ_0 and u appear in the product $\sigma_0\, u_+$, perturbations on σ_0 and u on classical indicators of the cardiac activity can be very similar.

5 Conclusion

Using a one-dimensional analogy with a deformable cylinder, a model of the excitation/contraction coupling in the myocardium is presented. The mathematical analysis of this model has been investigated in [16]. In this work, we have detailed the modeling. With numerical simulations we have also shown the ability of the proposed model to reproduce realistic cardiac cycles. The numerical aspects arising from the simulation of the proposed model are also detailed.

Even if the obtained results are in good agreement with the classical indicators of the cardiac function available in the literature, a realistic three-dimensional model including coronary perfusion

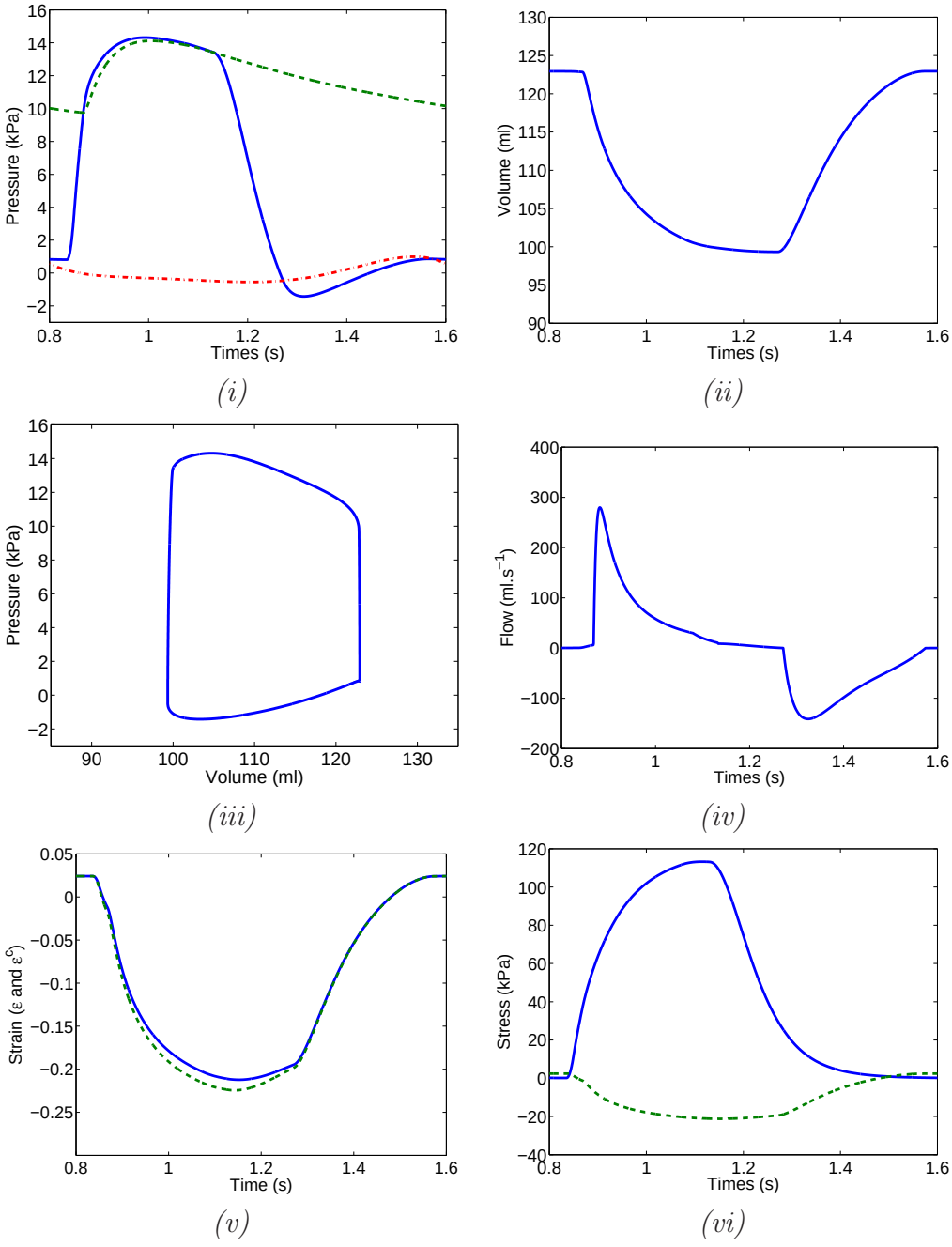

Figure 9: Global indicators of the cardiac function over a cardiac cycle. *(i)* ventricular (—), arterial (- -) and auricular (-.) pressures. *(v)*: total strain ε (—) and contractile strain ε^c (- -) at half-length of the piston. *(vi)*: contractile stress σ^c (—) and passive stress $\sigma^p = f_p(\varepsilon)$ (- -) at half-length of the piston.

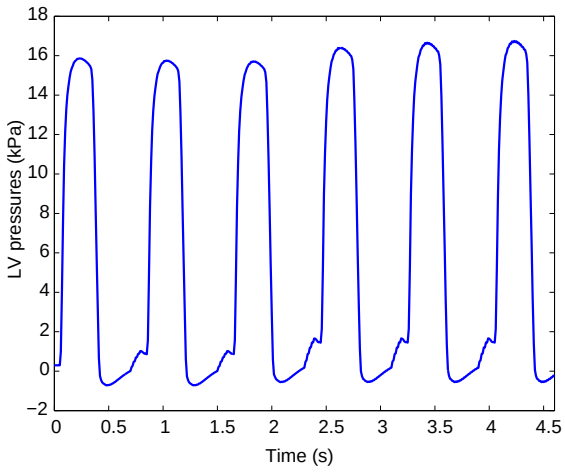

Figure 10: Pressure in the ventricular cavity over 6 cycles; a modification of σ_0, k_0 and u is introduced at the beginning of the fourth cycle.

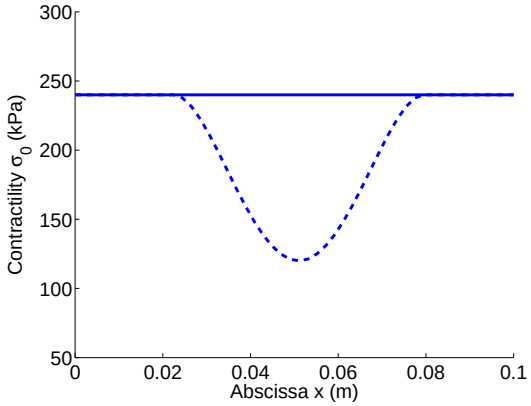

Figure 11: Variations of $\sigma_0(x)$ for $x \in [0, \ell]$. The solid line corresponds to the reference situation and the dashed one to the pathological case.

α	1
$P_{\rm at}(0)$	1 (kPa)
$P_{\rm ar}(0)$	10 (kPa)
σ_0	2.4 10^5 (Pa)
k_0	1.2 10^5 (Pa)
μ_c	200 (Pa.s^{-1})
μ	100 (Pa.s^{-1})
c_0	3 (m.s^{-1})
E_s	5 10^6 (Pa)
ℓ	0.1 (cm)
S	5 10^{-3} (m^2)
$K_{\rm p}$	10^{-1} (m^4.kg^{-1}.s)
$K_{\rm ar}$	300 (m^4.kg^{-1}.s)
$K_{\rm at}$	300 (m^4.kg^{-1}.s)
C	87 10^{-4} (l.Pa^{-1})
R_p	1.15 10^{-6} (Pa.l^{-1}.s)
τ	0.01 (s)
T	0.8 (s)
I^c	$[0.7, 0.8]$
$\bar{v}$	-30 (mV)
β_1	20
β_2	20
λ_1	1 (kPa)
λ_2	1 (kPa)
$\bar{\varepsilon_1}$	0
$\bar{\varepsilon_2}$	-0.25
h	0.25
ρ	1 (kg.m^3)
δP_0	0.5 (kPa)

Table 1: Values of the parameters used for the reference situation.

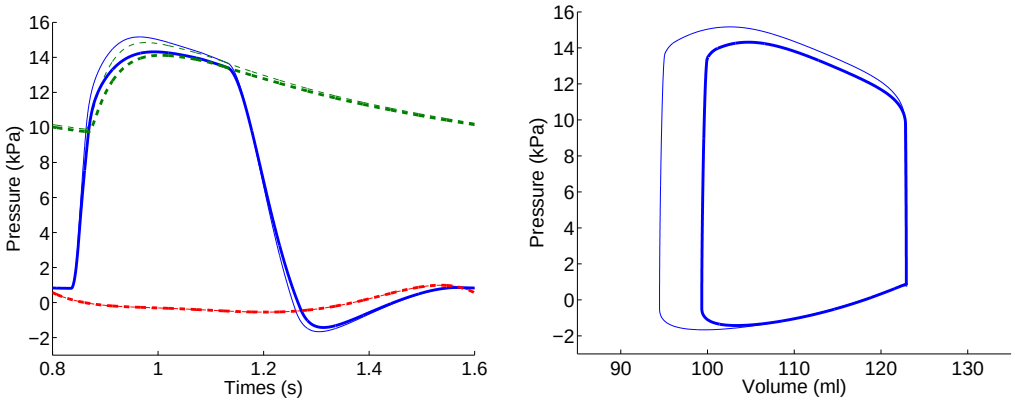

(i) *(ii)*

Figure 12: *(i)*: the ventricular (—), arterial (- -) and auricular (-.) pressures, the thick lines correspond to the pathological case and the thin ones to the reference situation. *(ii)*: the two corresponding PV loops.

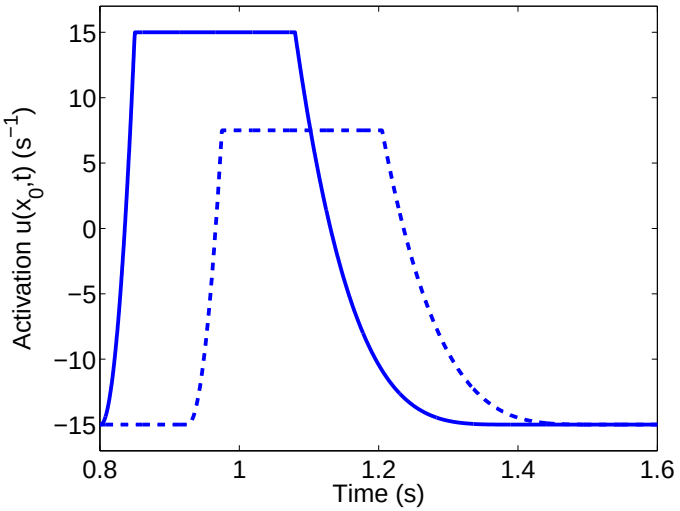

Figure 13: Activation $u(x_0, t)$ for $x_0 = \frac{\ell}{2}$, the dashed line correspond to the modified activation and the solid one to the reference activation.

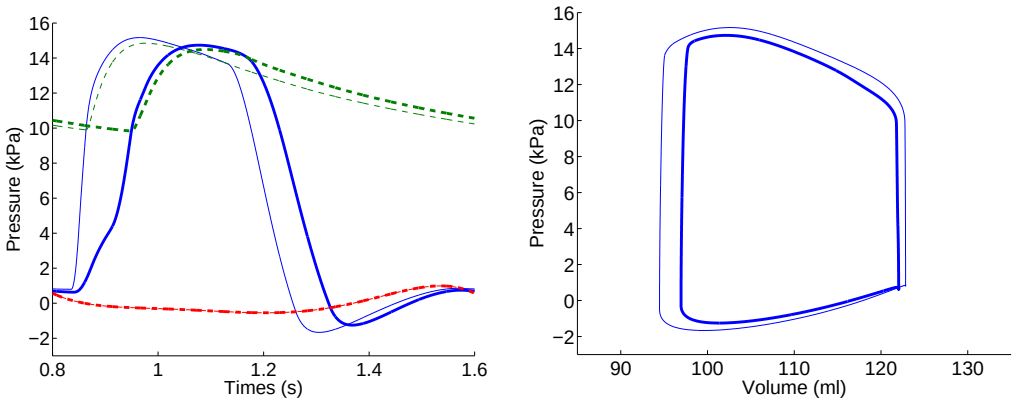

Figure 14: The thick line corresponds to the pathological case and the thin one to the reference situation. *(i)*: the pressures variations along a cardiac cycle and *(ii)*: the two corresponding PV loops.

needs to be developed and several regulatory mechanisms at the mechanical level or at the activation level (mechano-electric feedback) have now to be taken into account. These aspects are under investigation.

References

[1] H.D. Alber. *Materials with Memory: Initial-Boundary Value Problems for Constitutive Equations and Internal Variables*. Springer-Verlag, Berlin, 1998.

[2] R. Aliev and A.V. Panfilov. A simple two-variable model of cardiac excitation. *Chaos, Solitons and Fractals*, 7:293–301, 1996.

[3] A.P. Avolio. Multi-branched model of the human arterial system. *Med. Biol. Eng. Comput.*, 18(6):709–718, 1980.

[4] J. Bestel. *Modèle différentiel de la contraction musculaire contrôlée. Application au système cardio-vasculaire*. PhD thesis, University Paris IX Dauphine, 2000.

[5] J. Bestel, F. Clément, and M. Sorine. A biomechanical model of muscle contraction. In *Lectures Notes in Computer Science*, volume 2208. Eds W.J. Niessen and M.A. Viergever, Springer-Verlag, 2001.

[6] J.E. Bischoff, E.M. Arruda, and K. Grosh. Measurement of orthotropic material properties and constitutive modelling of soft tissue. In *Bioengineering Conference*. ASME, 2001.

[7] M. Brokate and Sprekels J. *Hysteresis and Phase transitions*. Springer-Verlag, New York, 1996.

[8] D. Chapelle, F. Clément, F. Génot, P. Le Tallec, M. Sorine, and J. Urquiza. A physiologically-based model for the active cardiac muscle. In *Lectures Notes in Computer Science*, volume 2230. Eds T. Katila, I.E. Magnin, P. Clarysse, J. Montagnat, J. Nenonen, Springer-Verlag, 2001.

[9] K. Djabella and M. Sorine. Differential model of excitation–contraction coupling in a cardiac cell for multicycle simulations. In *3rd European Medical and Biological Engineering Conference.*, Prague, 2005.

[10] P. Hunter, B. Smaill, and M. Nash. An orthotropic constitutive law for myocardium. In *Second World Congress of Biomechanics*, 1994.

[11] P. J. Hunter, A. D. McCulloch, and H. E. D. ter Keurs. Modelling the mechanical properties of cardiac muscle. *Progress in Biophysics and Molecular Biology.*, 69:289–331, 1998.

[12] P.J. Hunter, M.P. Nash, and G.B. Sands. Computational electromechanics of the heart. In *Computational Biology of the Heart*, pages 345–407. A.V. Panfilov and A.V. Holden Eds, John Wiley & Sons, 1997.

[13] A.F. Huxley. Muscle structure and theories of contraction. In *Progress in Biophysics and Biological Chemistry*, volume 7, pages 255–318. Pergamon press, 1957.

[14] A.M. Katz. *Physiology of the Heart.* Raven Press, 1992.

[15] J. P. Keener and J. Sneyd. *Mathematical Physiology.* Springer-Verlag, New-York, 1998.

[16] P. Krejčí, J. Sainte-Marie, M. Sorine, and J.M. Urquiza. Solutions to muscle fiber equations and their long time behaviour. *Nonlinear Analysis: Real World Analysis, In Press, Available online*, 2005.

[17] D.A. MacDonald. *Blood Flow in Arteries.* Edward Harold Press, 1974.

[18] I. Mirsky and W.W. Parmley. Assessment of passive elastic stiffness for isolated heart muscle and the intact heart. *Circul. Research*, 33:233–243, 1973.

[19] A. Monti, C. Médigue, and M. Sorine. Short-term modelling of the controlled cardiovascular system. *ESAIM Proc.*, 12:115–128, 2002.

[20] M. Pennacchio, P. Colli Franzone, L. Guerri, and B. Taccardi. A bidomain explanation of the multiple waveforms in electrograms. In *XXVII International Congress on Electrocardiology.*, Rome, 2000.

[21] M. Renardy, W.J. Hrusa, and J.A. Nohel. Mathematical problems in viscoelasticity. *Pitman Monographs and Surveys in Pure and Applied Mathematics*, 35, 1987.

[22] J. Sainte-Marie, D. Chapelle, R. Cimrman, and M. Sorine. 3D modeling and estimation of the cardiac electromechanical activity. *submitted to journal: Computers and Structures*, 2005.

[23] N. Stergiopulos, B.E. Westerhof, and N. Westerhof. Total arterial inertance as the fourth element of the windkessel model. *Am. J. Physiol.*, 276:H81–H88, 1999.

[24] T.P. Usyk, R. Mazhari, and A.D. McCulloch. Effect of laminar orthotropic myofiber architecture on regional stress and strain in the canine left ventricle. *J. Elasticity*, 61:143–164, 2000.

[25] D.R. Veronda and R.A. Westmann. Mechanical characterization of skin-finite deformation. *Journal of Biomechanics*, 3:114–124, 1970.

[26] A. Visintin. *Differential Models of Hysteresis.* Springer Verlag, Berlin, 1994.

[27] N. Westerhof, F. Bosman, C.J. De Vries, and A. Noordegraaf. Analog study of the human systemic arterial tree. *J. Biomech.*, 2:121–143, 1969.

[28] A.Y.K. Wong. Mechanics of cardiac muscle based on huxley's model: mathematical simulation of isometric contraction. *J. Biomech.*, 4:529–540, 1971.

[29] J.Z. Wu and W. Herzog. Modelling concentric contraction of muscle using an improved cross-bridge model. *Journal of Biomechanics*, 32:837–848, 1999.

[30] G.I. Zahalak. A distribution moment approximation for kinetic theories of muscular contraction. *Mathematical Biosciences*, 55:89–114, 1981.